IMPACT: International Journal of Research in Engineering & Technology (IMPACT: IJRET)
ISSN(P): 2347-4599; ISSN(E): 2321-8843
Vol. 4, Issue 7, Jul 2016, 13-32

COMPARATIVE SPECTROSCOPIC AND ELECTROKINETIC STUDIES ON METHYLENE – BLUE ADSORPTION ON TO SAND AND BRICK FROM CENTRAL AFRICAN REPUBLIC

B. BAGOUA[1], E. FOTO[2], O. ALLAHDIN[3], M. WARTEL[4], J. MABINGUI[5] & A. BOUGHRIET[6]

[1,2,3,5]Chaire Unesco ―Sur la Gestion de l'eau, Laboratoire Hydro sciences Lavoisier, Université de Bangui, Faculté des Sciences, République Centrafricaine Central Africa

[4,6]Université Lille 1, Laboratoire LASIR (UMR CNRS 8516), Equipe Physico-chimies de l'Environnement. Bât. C8 2ème Etage, Villeneuve d'Ascq Cedex, France

ABSTRACT

Chemical properties of local sand and brick from Central African Republic were determined by using the following techniques: ESEM/EDS, ^{1}H, ^{23}Na and ^{29}Si MAS NMR, CHNS, and ICP-AES. From batch experiments, sand and brick samples were tested for the adsorption of methylene blue (MB) in aqueous media. The experimental data were well correlated by both the Langmuir and Freundlich models. Brick adsorbents were developed with better adsorption for the removal of MB from aqueous solutions than sand. Hydroxylation and dealumination of the brick with HCl, followed by a deposition of iron oxyhydroxide, significantly improved its MB adsorption capacity. Structural and morphological characterization further proved that coated brick had better BET surface area and porosity than sand. Electrokinetic studies on sand and brick samples confirmed that electrostatic interaction is indeed the potential mechanism contributing to the enhanced MB adsorption on these adsorbents. Spectroscopic analyses showed that the enhanced adsorption capacity of treated brick was intimately related to the generation of sodic surface sites: $\equiv S{-}O^{-}Na^{+}$ (with S = Fe, Al, and Si) that favor the uptake of a cationic dye like methylene blue *via* electrostatic forces at the solid – water interface.

KEYWORDS: Sand, Brick, Adsorption, Methylene Blue, Zeta Potential, Isotherms

1. INTRODUCTION

The removal of dyes from wastewaters becomes a relevant environmental issue because these synthetic compounds are difficult to biodegrade, can affect aquatic ecosystems (by diminishing light penetration and thereby photosynthesis process), and can cause damage to human beings due to their toxic, mutagenic or carcinogenic characteristics. Numerous adsorbents like clays [1-4], fly ash [5-8], alumina [9-11], activated carbon [12-15], biosorbents [16, 19], and polymers [20-24], have been reported for the removal of dyes from aqueous solutions. But, their cost, abundance, accessibility or synthesis often limits economically their use. In contrast, natural minerals like sand and brick (a composite mainly composed of sand and clays and, to a lesser extent, iron oxides) have more potential as inexpensive and environmental friendly adsorbents due to their greater abundance worldwide, much lower cost, chemical and physical stability, and high permeability that facilitate the flow of water in sand/brick beds. Sand is commonly used as filter media in wastewater-treatment plants for the removal of turbidity, SS (suspended solids), COD (chemical oxygen demand), BOD (bio-chemical oxygen demand), and coliforms bacteria through physical / microbiological processes ([25-27] and

references therein). Sand filters are also known to be an economical method which necessitates less skilled manpower due to its simplicity. Sand was also used in the past as an adsorbent in laboratory scale experiments for the removal of, for instance: inorganic ions [28, 29], and dyes [30-32] from water. As for the brick, its adsorption characteristics were employed in the removal of various ionic species: (i) ***inorganic anions*** like: phosphates alone [33], or phosphates + nitrates + chlorides [34], fluorides [35]; (ii) ***metallic ions*** like: Hg(II) [36], Zn(II) [37], Cr(VI) [38], both Cr(VI) and Ni(II) [39], or Ni(II) alone [40]; and (iii) ***organic compounds*** like: detergent composed of surfactants (linear alkyl benzene sulfonate + alkyl sulfate) [34]), methylene blue [41, 42], dye basic blue *41* [43].

The objective of the present work was to evaluate the ability of locally available sand and brick in Central African Republic (C.A.R.) for the elimination of methylene blue (MB) from aqueous solutions. The study was carried out with the aim to compare the adsorption performances of these materials toward a cationic organic species, MB. Batch experiments were performed under different conditions of initial dye concentration, and adsorption isotherms were determined by testing two mathematical models: Freundlich and Langmuir. The brick was afterwards modified by different chemical surface treatments in a manner that these significantly improved its capability to uptake MB from water. Elemental compositions of sand and brick samples were determined by the ICP-AES and CHNS techniques, and the nature of adsorption sites present at their surfaces was investigated by ESEM/EDS and ^{1}H, ^{23}Na and ^{29}Si MAS NMR. Zeta measurements were performed on sand and brick samples with the aim of assessing the effects of chemical surface changes on the adsorption performance of the adsorbents studied.

2. MATERIALS AND METHODS

2.1 Adsorbents preparation

The sand and brick samples used in this study were obtained from Bangui region in the Central African Republic. Two types of sand were used in this work: one collected in soils near Bangui city; the other in Oubangui - river bed. X-ray diffraction and chemical analysis were performed on these materials: sand is mainly composed of quartz; and brick of the following minerals: ~ 60-65 wt % quartz; ~ 20-25 wt % metakaolinite ($2SiO_2.Al_2O_3$); 4-5 wt % illite; ≤ 4 wt % iron oxides / hydroxides; and ≤ 3 wt % feldspar + mica + biotite. Before use, several physical / chemical treatments were carried out on the raw brick. First, it was broken into grains and sieved with sizes ranging from 0.7 to 1.0 mm. Second, the resulting particles were leached with a 6M HCl solution at 90°C for 6 hours. Third, a deposition of FeOOH onto HCl - treated brick was performed by a precipitation of iron (III) (by using a 0.25M Fe^{3+} ions solution) with NaOH solutions (6M and 1M) at around pH 7.4. As for the sand samples, they were sieved into five types of grain sizes: 0.2 – 0.4; 0.4 – 0.6; 0.6 – 1.0; 1.0 – 1.4 mm; and > 1.4 mm.

2.2. Chemicals

All chemicals employed in the experiments were analytical grades. Sodium hydroxide and hydrochloride acid were supplied by DISLAB (France). The salt $Fe(NO_3)_3{\cdot}H_2O$ was purchased from Prolabo, and methylene blue from VWR Chemicals (DISLAB).

2.3. Chemical Attack and Procedure

All chemical attacks of sand and brick samples were made with 2M nitric acid at 90°C for 2 hours. The recovered solutions were analyzed for element contents using Inductively Coupled Plasma - Atomic Emission Spectroscopy

(ICP-AES); model Varian Pro Axial View.

2.4. Spectroscopic Analyses

2.4.1 Electron Microscopy analysis__ Micrographs of representative specimens of sand and brick were recorded by using an environmental scanning electron microscope (ESEM, Quanta 200 FEI). Elemental analysis was performed using ESEM/EDS (ESEM, model: QUANTA–200–FEI, equipped with an Energy Dispersive X-Ray Spectrometer EDS X flash 3001 and monitored by QUANTA–400 software elaborated by Bruker). ED's measurements were carried out at 20 kV at low vacuum (1.00 Torr) and the maximum pulse throughput was 20 kcps. Different surface areas ranging from 0.5 to 3.5 mm² were targeted on sand or brick grains and examined by ESEM/EDS. Atomic quantifications and mathematical treatments were undertaken using QUANTA-400 software in order to determine the averaged elemental composition of the surface brick /sand and to detect chemical / elemental variability's.

2.4.2 NMR MAS analysis__ ^{1}H and ^{23}Na MAS NMR spectra were recorded at 800 and 211.7 MHz, respectively, on a 18.8 T Bruker Avance III spectrometer equipped with a Bruker 3.2 mm probe-head. ^{1}H MAS NMR analyses were performed at a spinning frequency (ν_{rot}) of 20 kHz with a pulse length of 3.25 µs ($\pi/2$ flip angle), 64 transients and a recycle delay (rd) of 5 s. ^{23}Na (I = 3/2) MAS NMR analyses were performed at a ν_{rot} of 20 kHz with a pulse length of 1 µs (~ $\pi/5$ flip angle), 1024 transients, and 2 s rd. To characterize the local structure around silicon atoms in the brick samples, ^{29}Si MAS NMR spectra were acquired at 79.5 MHz on a Bruker AVANCE I 9.4 T spectrometer equipped with a Bruker 7.0 mm probe-head. ^{29}Si MAS NMR spectra were recorded with a ν_{rot} of 4 kHz, a pulse length of 5 µs ($\pi/2$ flip angle), 256 transients and 30 s rd. All the ^{1}H, ^{23}Na, and ^{29}Si chemical shifts were referenced as 0 ppm to TMS, NaCl solution (1 M), and TMS, respectively.

2.5. Batch Experiments

Adsorption-isotherms studies were performed in ten 100mL-flasks _each one containing 2g of brick pellets_ in which were added 50 mL of a methylene blue (MB) solution having a concentration ranging from 10^{-6} to $5x10^{-5}$ M. These flasks were placed on a mechanical shaker (as mentioned above) and gently shaked at a speed of 120 rpm. Preliminary sorption experiments showed that a reaction time of 4 hours at a temperature of 17°C ± 1°C was sufficient for the system to attain thermodynamic equilibrium. Afterwards, suspensions were filtered and the recovered solution was analyzed to determine MB concentrations using UV-Visible spectrometry at a wavelength of 644 nm. The quantity of MB adsorbed on to sand or brick, noted Q_e (in mg/g) was assessed from the difference between the initial and the equilibrium contents of MB (in the liquid phase), which was divided by the mass of suspended material. It should be noted that all these experiments were at least triplicate and data were averaged.

3. RESULTS AND DISCUSSIONS

3.1 Isotherm Models

Studies of adsorption isotherms are very important to gain information about adsorption performances of sand and brick toward MB. Langmuir and Freundlich isotherms models were applied in this work to fit the equilibrium adsorption data of MB on to different samples of sand and brick. For that, the adsorption isotherms of MB on to sand and brick were determined in the range of MB concentration between 10^{-6} and $5x10^{-5}$ M. The amount of dye removed per gram of adsorbent was calculated from the equation:

$$Q_e = \frac{(C_o - C_e)V}{m} \quad (1)$$

In which Qe (mg/g) is the amount of MB adsorbed at equilibrium; Co and Ce represent the initial and at equilibrium dye concentrations (mg/L; and V and m are the volume of the solution (L) and mass of adsorbent (g), respectively. For instance, figure 1 displays the plots of Qe versus Ce which were obtained in the removal of MB from water with different grains sizes of sand.

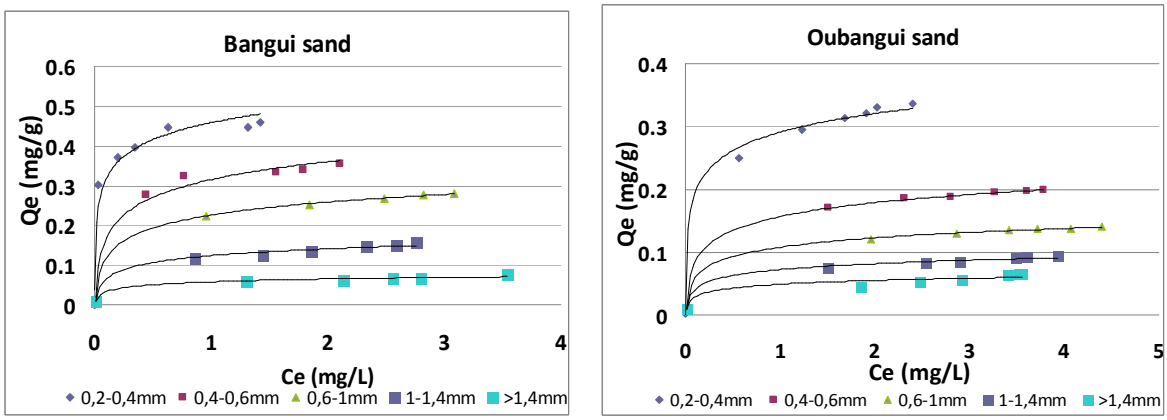

Figure 1: Variation of the Amount of MB Adsorbed at Equilibrium on to Sand Samples (Qe; Mg/G) as Function of the MB Concentration at Equilibrium in the Liquid Phase (Ce; Mg/L)

*Langmuir isotherm*__ This mathematical model assumes that the adsorbent possesses homogeneous (monolayer) adsorption surfaces. It is represented by the following equation [44]:

$$Q_e = \frac{Q_{max}.K_L.C_e}{1 + K_L.C_e} \quad (2)$$

Where C_e is the equilibrium aqueous MB concentration (mg/L); Q_e the amount of MB adsorbed per gram of adsorbent at equilibrium (mg/g); Q_{max} and K_L are the Langmuir constant related to the maximum adsorption capacity (mg/g) and energy of adsorption (L/mg), respectively. The linear form of the Langmuir expression is given by:

$$\frac{C_e}{Q_e} = \frac{1}{K_L.Q_{max}} + \frac{C_e}{Q_{max}} \quad (3)$$

The plots of C_e/Q_e versus C_e are linear for all studied adsorbents (see Figure 2).

*Freundlich isotherm*__ This mathematical model is employed for heterogeneous adsorption surfaces, and is expressed as [44, 45]:

$$Q_e = K_F.Ce^{1/n} \quad (4)$$

Where K_F is the Freundlich constant representing the multilayer adsorption capacity; and n is a constant depicting the adsorption intensity. The linear form of the Freundlich expression is given by:

$$Log(Q_e) = Log(K_F) + (1/n)\ Log(C_e) \quad (5)$$

The plots of Log (Q_e) versus Log (C_e) are linear for all studied adsorbents (see Figure. 2).

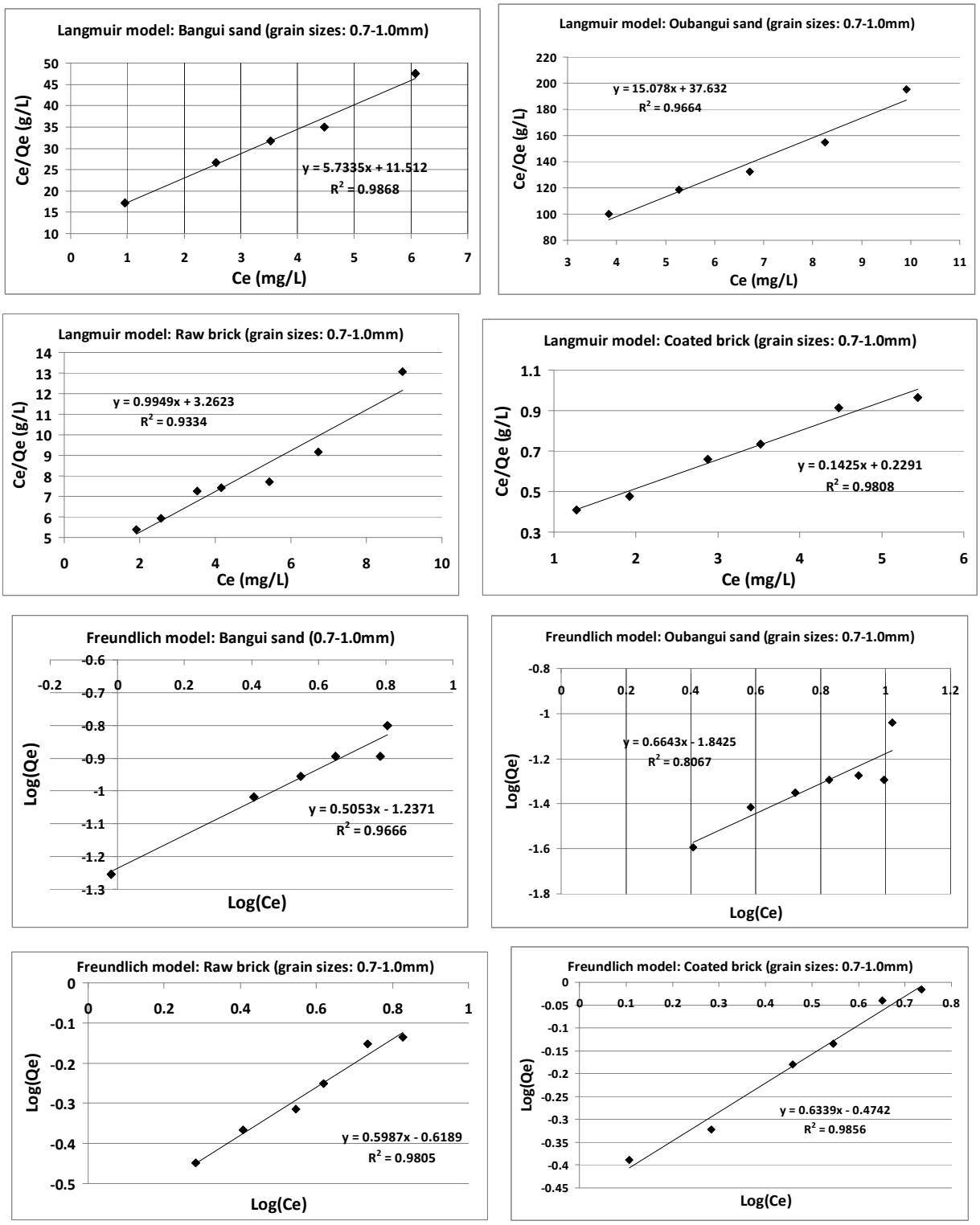

Figure 2: Langmuir and Freundlich Isotherms for MB Uptake by Sand and Brick Samples from Aqueous Solutions

*Adsorption isotherms analysis*__ A detailed analysis of the correlation coefficients (R^2) from Table 1 showed that Langmuir and Freundlich models adequately predicted the experimental data well for the adsorption of MB on to sand and

brick.

Table 1: Langmuir and Freundlich Parameters for MB Uptake by Sand and Brick Samples

Adsorbent	Langmuir			Freundlich		
	Q_{max} (Mg/G)	K_L (L/Mg)	R^2	K_F (L/G)	N	R^2
Oubangui sand						
0.2 - 0.4mm	0.38	3.22	0.9985	0.58	5.14	0.9994
0.4 - 0.6mm	0.22	2.00	0.9986	0.45	5.88	0.9908
0.6 - 1.0mm	0.16	1.43	0.9991	0.38	5.17	0.9952
1.0 – 1.4mm	0.11	1.43	0.9942	0.31	5.22	0.9786
>1.4mm	0.10	0.40	0.9999	0.22	1.78	0.9865
Bangui sand						
0.2 – 0.4mm	0.47	17.66	0.9989	0.70	9.09	0.9726
0.4 – 0.6mm	0.37	6.65	0.9974	0.59	4.68	0.9778
0.6 - 1.0mm	0.32	2.24	0.9975	0.52	4.36	0.9885
1.0 – 1.4mm	0.22	1.55	0.9929	0.39	3.01	0.9752
>1.4mm	0.10	1.46	0.9854	0.29	7.73	0.9548
HCl-treated sand						
0.6 – 1.0mm	0.04	0.54	0.908	0.14	0.91	0.9777
Raw brick						
0.7 - 1.0mm	1.005	3.05	0.9394	0.539	1.676	0.9810
HCl-treated brick						
0.7 – 1.0mm	0.788	0.024	0.925	0.196	1.235	0.9677
Coated brick						
0.7 – 1.0	7.018	0.622	0.9808	0.622	1.578	0.985

It is however interesting to note that for both sand and coated brick Langmuir model presents some better correlation coefficients ($0.9808 < R^2 < 0.9986$) than those from Freundlich model ($0.9548 < R^2 < 0.9994$). In other words, Langmuir isotherm was found to be more applicable to the experimental data of MB, indicating the formation of monolayer coverage of the adsorbate at the surface of sand and coated brick.

Figure 3 shows the comparison of adsorption performances obtained in this work for sand and brick samples.

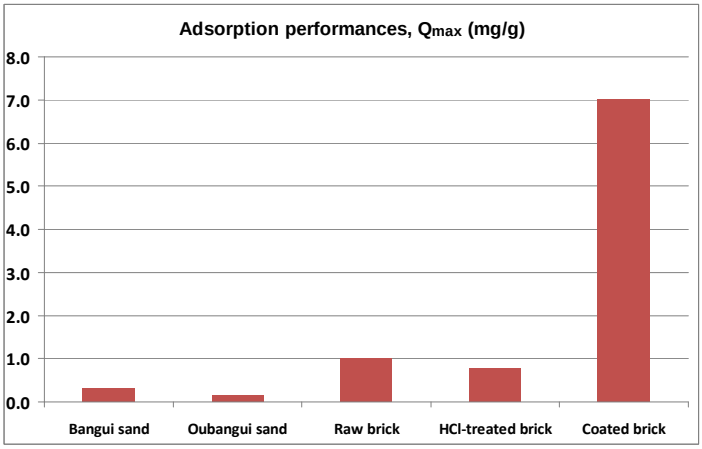

Figure 3: Comparison of MB Adsorption Performances Obtained for Different Sand and Brick Adsorbents

In what follows, we first tried to identify the phase(s) and functional groups which were presumed to be implicated at the adsorbent-water interface during the MB-adsorption process.

3.2 Chemical Properties of Sand and Brick from C.A.R

Sand__ ICP-AES analyses of solutions recovered after total acid attack of sand samples revealed the presence of aluminum, and to a lesser extent, iron in addition to silicon which is the major element (with oxygen) in the chemical structure of natural quartz.

The ESEM micrograph of a sand grain (Figure 4) displays regions of different contrasts with white and grey tones which indicate the diversity of compounds forming the sample.

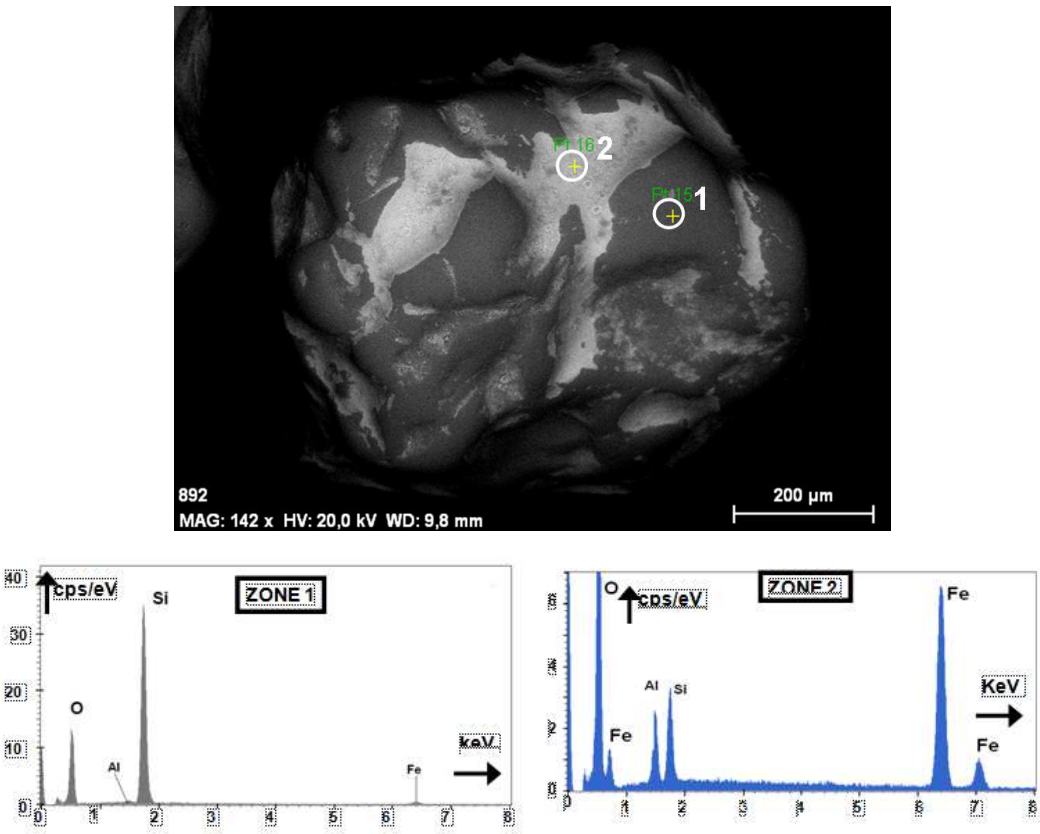

Figure 4: ESEM Image of a Raw–Sand Grain, and EDS Spectra of two Targeted Surfaces (Zones 1 and 2)

In this typical ESEM image (Figure 4), the targeted surfaces are mainly composed of O and Si on dark zones (in which Al and Fe are present at low levels) and O, Fe, Si and Al on light zones, as shown in the two EDS spectra of Figure 4. It can be concluded that sand surfaces contain roughly both SiO_2 (with some traces of iron oxides and clays) in dark zones and iron oxides and clays in light zones.

ESEM/EDS micro-observation with a cross-section of a sand grain indicated increasing levels of both iron and aluminum alongside a light-grey zone shown in the micrograph of Figure 5, whereas levels of silicon decreases in dark zones (Figure 5).

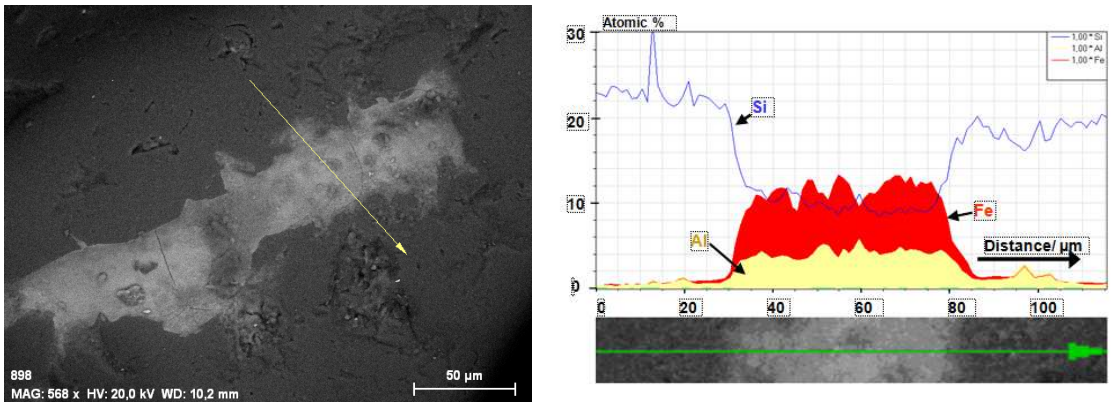

Figure 5: ESEM/EDS Micro-Observation with a Cross-Section of a Raw–Sand Grain Showing the Levels of Al, Fe and Si Atoms

This observation suggested that iron oxides are associated with clays at sand surfaces.

To know whether or not the aluminosilicates and iron oxides present at the surface of Bangui sand played a role in the removal of MB from water, the adsorption capacity (Q_{max}) was plotted against Al and Fe amounts see Figure 6. As can be seen in this figure, no correlation was found between Q_{max} and Al and Fe, suggesting that these surface phases are not implicated in the MB-adsorption process.

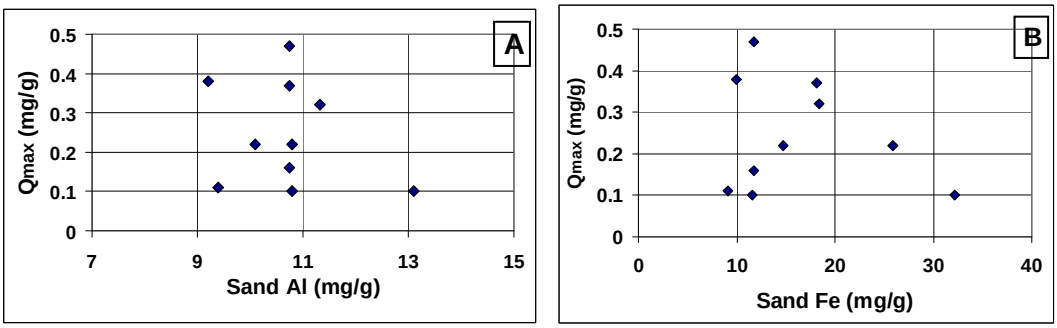

Figure 6: Evolution of the MB–Adsorption Capacity of the Sand (Qe; Mg/G) as a Function of Al Content (Mg/G) __ (A); and Fe Content (Mg/G) __ (B)

Moreover, the CHNS technique permitted us to confirm the presence of organic matter (OM) which is coated on to sand grains: the content of organic carbon (OC) varied from 0.189 to 0.876 g per kg of sand, see Table 2.

Table 2: Organic–Carbon Contents (G/Kg) in Raw–Sand Samples with Different Grain Sizes

	Organic carbon (g/kg)	
	Bangui sand	*Oubangui sand*
0.2 – 0.4mm	0.876	0.834
0.4 – 0.6	0.696	0.436
0.6 – 1.0	0.446	0.275
1.0 – 1.4	0.331	0.283
> 1.4	0.189	0.302

The MB–adsorption capacity was plotted against the OC value for different Bangui–sand samples (see Figure 7).

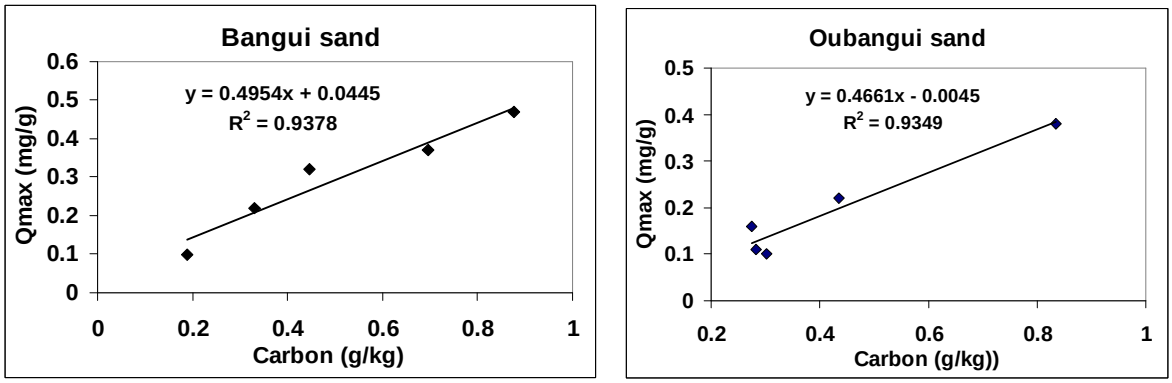

Figure 7: Variation of the MB–Adsorption Capacity (Q_{max}; Mg/G) of two Raw Sands (one from Bangui Region and the Other from Oubangui River-Bed) as a Function of Organic Carbon Content (G/Kg) Present in These Adsorbents

A straight line was found with a correlation coefficient $R^2 \approx 0.94$-0.93. This finding proved the importance of organic matter (fulvic and/or humic acids) in the binding of MB at the sand surface. It was previously suggested that MB can react with both anionic and aromatic groups of humic acids through ion exchange and π - π interactions [46, 47]. However, the nature of organic matter at sand surfaces was not investigated here, and mechanistic aspects were not addressed as well.

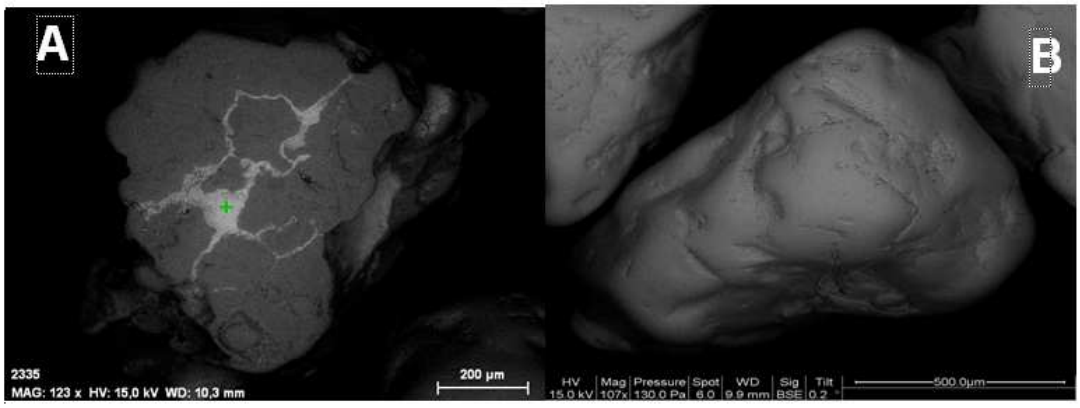

Figure 8: ESEM Micrographs of a Sand Grain: Before__ (A); and After an Acid Treatment with a 6M Hcl Solution at 90°C for 3 Hours__ (B)

It is worth noting that an acid treatment of raw sand with a 6M HCl solution at 90°C for 3 hours led to the elimination of all the coatings on quartz surfaces (as shown above in Figure 8), and consequently, the MB–adsorption capacity of resulting grains was found to decrease strongly from 0.32 to 0.04 mg/g (see Table 1).

Raw brick__ The ESEM micrograph of raw brick exhibits highly porous and non-uniform textural surfaces with major fissures and cracks, except for quartz crystals (not shown here). Detailed ESEM/EDS analyses were performed sporadically on raw – brick particles (not shown here), and as a whole micro-analytical data showed that the compositions of targeted regions are mainly: Si and O derived from SiO_2 in the crystalline form of quartz; Al, Si and O from (metakaolinite) aluminosilicates; and to a lesser extent Fe-rich deposits indicating the presence of iron oxides.

HCl-treated brick__ the ^{29}Si MAS NMR spectrum consists of three resolved resonances centered at -91, -102, -

111 ppm (in addition to the resonance of quartz silicons at -107 ppm), as pointed out previously [48]. These signals were ascribed respectively to: (i) Q^3 Si $(SiO)_{3OH}$; (ii) Q^3 Si $(SiO)_2(AlO)OH$ and/or Q^2 $Si(SiO)_2(OH)$; (iii) Q^4 ^{29}Si nuclei with no "–OH" functions in their immediate proximities [48]. After spectral deconvolution, the ^1H MAS NMR spectrum contains four magnetic resonances which were attributed to: (i) isolated silanols and aluminols at ~1.8 and ~2.9 ppm [48-50]; (ii) H_2O bound to aluminosilicates [49] and/or physisorbed water at varying degrees of hydrogen bond strength [51]; and (iii) H-bonded water and H-bonded silanol at 6.5-7.0 ppm [48-51].

Iron-oxihydroxide-coated brick__ Figure 9 shows the ESEM micrograph of coated-brick specimens. The ESEM/EDS technique revealed that silicon, oxygen, aluminum and iron are the major elements.

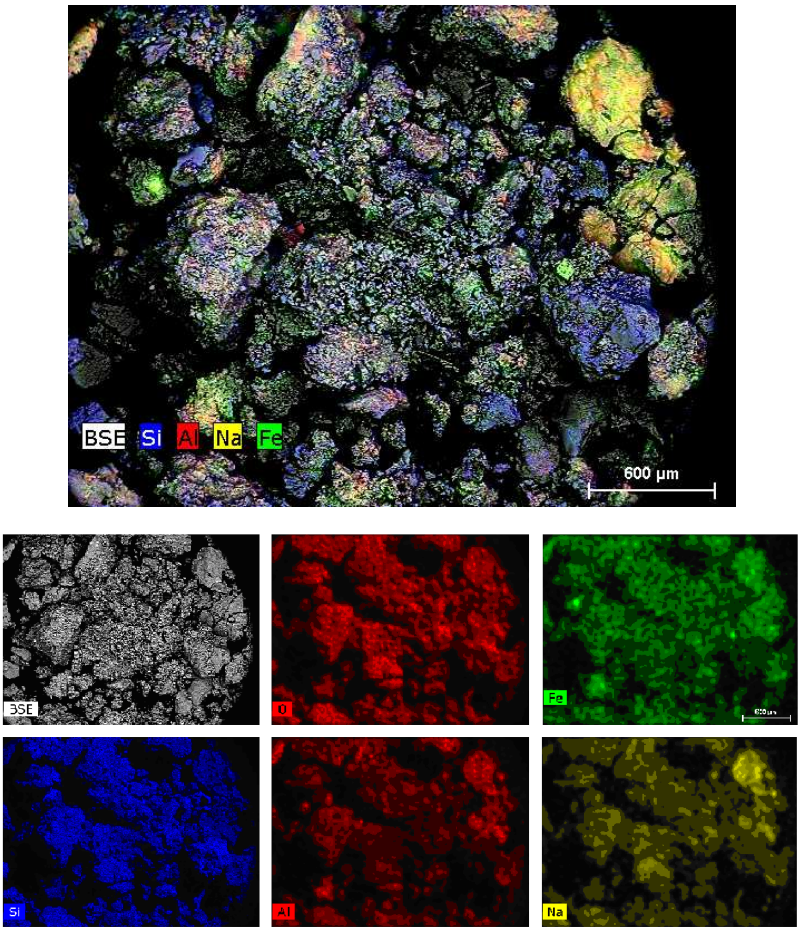

Figure 9: ESEM/EDS Mapping: Spatial Distribution of Al, Fe, Na and Si on Coated Brick

From EDS mapping images (Figure 9), the spatial distribution of Al, Fe, Na and Si on a targeted surface of coated brick permitted us to localize Si-rich particles, Al-rich aggregates and Fe-rich deposits. These three zones are mainly composed of quartz, aluminosilicates and iron oxyhydroxide, respectively. We greatly suspect the involvement of an attachment of iron to clay surfaces with the formation of Al-Si-Fe-O associations (as clusters) during the coating procedure, as pointed out by Cismasu et al. [52].

The ^1H MAS NMR spectrum (not shown here) consists roughly of a (badly resolved) broad signal which is largely lower than that observed for HCl-treated brick. This signal attenuation results from the neutralization of hydroxyl groups

by sodium hydroxide at the brick surface according to:

$$\equiv X–OH + Na^{+}OH^{-} \leftrightarrow \equiv X–O^{-}\ Na^{+} + H_2O \quad (6)$$

The occurrence of sodium atoms at the brick surface was confirmed both by the EDS mapping image of this element (see Figure 9) and ^{23}Na MNR (not shown here).

3.3 BET Analyses of Sand and Brick from C.A.R

Surface area and porosity of sand and brick samples are important characteristics for their applications as adsorbents since they determine their accessibility of MB molecules to the active sites described above. Their BET surface areas and porosity were investigated based on nitrogen adsorption-desorption isotherms at 77 °K. BET data are listed in Table 3.

Table 3: Specific Surface Area, Pore Volume and Average Pore Diameter Measured on Sand and Brick Samples with Different Grain Sizes

Adsorbent	Specific Surface Area (BET), M^2/G	Pore Volume, Cm^3/G	Average Pore Diameter, Å
Bangui sand			
0.2 – 0.4mm	1.5	0.002	38.9
0.4 – 0.6	2.0	0.002	40.4
0.6 – 1.0	2.4	0.002	40.4
1.0 – 1.4	3.0	0.002	40.4
> 1.4	4.1	0.004	40.5
Oubangui sand			
0.2 -0.4mm	0.7	0.001	39.6
0.4 – 0.6	2.9	0.002	40.4
0.6 – 1.0	2.9	0.001	39.7
1.0 – 1.4	2.2	0.002	40.4
>1.4	2.0	0.001	39.4
Raw brick			
0.7 – 1.0mm	76	0.150	160
HCl-treated brick			
0.7 – 1.0mm	96.7	0.230	161
Coated brick			
0.7 – 1.0mm	49.1	0.210	203

As a whole, the BET surface areas of sand and brick samples were respectively 0.7–4.1 m^2/g and 49.1–96.7 m^2/g, and pore volumes were respectively 0.001–0.004 cm^3/g and 0.150–0.230 cm^3/g, while average pore diameters varied from 38.9 to 40.5 Å for sand samples and from 160 to 203 Å for brick samples. To summarize, the weak BET surface areas and porosities of sand samples suggested the difficult accessibility of MB molecules to the active sand sites, which is directly associated with their adsorption capacity; As for the raw brick, its specific surface area is about 76 m^2/g, which is from 20 to 100 orders of magnitude higher than those of the studied sands; After acid activation (with HCl 6 M at 90°C for 6 hours according to a hydroxylation/dealumination process), the surface areas and pore volumes of the activated brick increased respectively from 76 to 96.7 m^2/g and from 0.150 to 0.230 cm^3/g as a result of the generation of new hydroxyl groups (aluminol and silanol) at its surface, as described in section 3.2. However, the surface area of HCl-treated brick decreased at 49.1 m^2/g by a deposition of iron oxy hydroxide on to its surface, while its average pore diameter increased from 161 to

203 Å and its pore volume barely changed from 0.230 to 0.210 cm^3/g. Changes in surface area and porosity obtained for coated brick were due to its aggregates morphology, which caused profound external surface roughness when compared to sand surfaces (see Figures 4, 8 and 9).

Following the detailed chemical characterization and BET analyses described in sections 3.2 and 3.3, the samples of sand and brick were subjected to electro kinetic tests. The zeta potential provides information on changes in the ionic surface properties of the solid particles suspended in water.

3.4 Electro kinetic Behavior

Zeta potential measurements were performed on sand and brick samples over a pH range from 2 up to 9 (Figure 10).

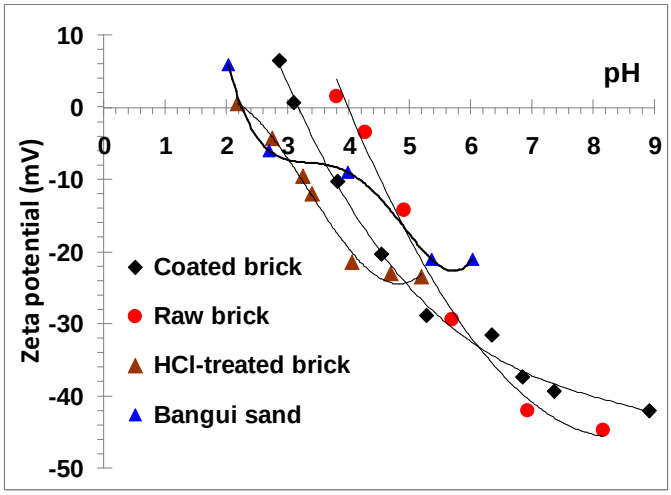

Figure 10: The Influence of Ph on the Zeta Potential of Different Adsorbents: Bangui Sand; Raw Brick; Hcl–Treated Brick; and Coated Brick

Electrokinetic data revealed a zeta potential reversion for both the sand and brick, from positive to negative, evidencing that the surface charge in these materials was affected by the medium pH. The observed electrokinetic properties could be attributed to surface protonation or de-protonation, depending mainly upon how hydroxyl (organic or mineral) groups on the surface of sand and brick interact with surrounding water molecules, H_3O^+ and OH^- ions.

As a whole, the zeta potential becomes positive at low pH ($pH < pH_{IEP}$) and negative at high pH for both materials due to their amphoteric nature. Thus, at low pH "hydroxyl" (organic and/or mineral) surface groups (noted ≡X–OH in the text) can react with protons as:

$$\equiv X\text{–}OH + H_3O^+ \leftrightarrow \equiv X\text{–}OH_2^+ + H_2O \quad (7)$$

And with the increase of the pH value, the zeta potential then decreases and becomes negative, revealing the deprotonation / dissociation of hydroxyl functions and generation of negative charges on the solid surface as:

$$\equiv X\text{–}OH + H_2O \leftrightarrow \equiv X\text{–}O^- + H_3O^+ \quad (8)$$

In this latter case, the cationic dye (MB) removal can be enhanced by strong electrostatic attraction between deprotonated groups (≡X–O^-) and positively charged $\rangle N^+$ groups of MB dye.

The curves of zeta potential versus pH, determined for the sand samples, are shown in Figures 10 and 11. Their isoelectric point (IEP) occurs at pH 2.2-2.3; their maximum zeta potential is +5 mV, and the minimum -23 mV. The IEP value indicates the pH at which the zeta potential becomes equal to 0, and the negative surface charges equilibrate the positive surface charges as well.

After the elimination of organic matter from the sand by heating at 500°C for 24 hours, the pH at the isoelectric point (pH_{IEP}) was found to increase from ~2.3 (before treatment) to ~3.5 (after treatment), see Figure 11.

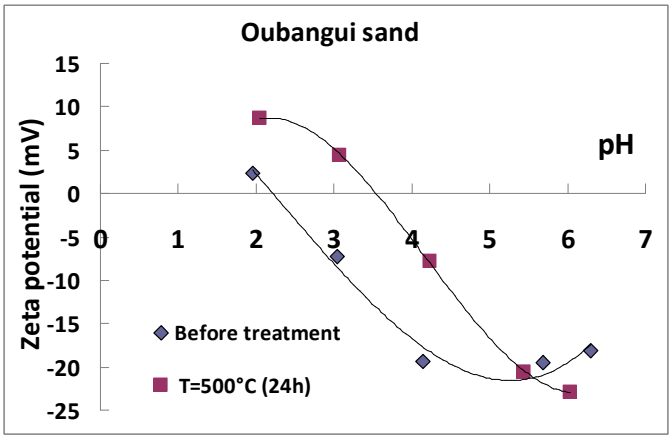

Figure 11: The Influence of Ph on the Zeta Potential of Oubangui Sand Before and After a Thermal Treatment at 500°C for 24 Hours

The pH_{IEP} for heated sand was approximate to the IEP values reported for quartz (2.8; [53, 54]), quartz+Fe^{3+} (~3; [55]) and most-studied SiO_2 specimens (2.6-3.8; [56]). The maximum zeta potential becomes +8.7 mV at pH 2.05, and its minimum -22.9 mV at pH 6.05. The observed shift in the pH_{IEP} toward a positive value for a binary-system of sand + HA after the heating procedure, seems then to be consistent with a loss of the electrokinetic properties of HA since the pH_{IEP} of humic acids is known to be ≤ 2 [53, 54].

The curve of zeta potential versus pH, determined for raw brick, is shown in Figure 10. Its isoelectric point (IEP) occurs at pH 4.0; and its minimum zeta potential is -44.7 mV at pH 8.15.

Note that some differences emerge concerning the electro kinetic properties of the sand and brick: *first* the pH_{IEP} of the sand is lower than that of the brick; and *second* at pH > pH_{IEP} the curve for the brick (Figure 10) lies below that of the sand over the whole range of pH > pH_{IEP} values. This latter finding indicated that the brick surface is more negatively charged in water, and thereby potentially better adsorbent of cations than the sand surface (see Figure 3), in agreement with batch experiments on MB adsorption reported in section 3.1.

For HCl–treated brick, the pH at the isoelectric point becomes lower (pH_{IEP} = 2.3; see Figure 10) than that of raw brick (pH_{IEP} = 4.0) as a result of the generation of new acid sites at the surface (silanol and aluminol). However, it was noticed that the adsorption performance of this material barely changes when compared to that of raw brick (Figure 2). Indeed, SiOH in hydroxylated brick (like in kaolinite) is weakly dissociated as:

$$\Xi SiOH + H_2O \rightarrow \Xi SiO^- + H_3O^+ \quad (9)$$

($pK_A \approx 4.0$ - 6.5 for silanols in kaolinite [57]);

And AlOH is much weakly dissociated as:

$$\Xi AlOH + H_2O \rightarrow \Xi AlO^- + H_3O^+ \quad (10)$$

($pK_A \approx 8.40 - 9.84$ for aluminols in kaolinite [57]).

After precipitating iron(III) on HCl-treated brick with iron sodium hydroxide, the pH at the isoelectric point for the resulting material becomes higher (pH_{IEP} = 3.2), and the minimum zeta potential is -42 mV at pH 8.9, see Figure 10. The observed shift in the zeta potential toward a positive value for the binary-system of brick + iron oxyhydroxide is consistent with previous observations on adsorption characteristics of montmorillonite clay modified with iron oxide with respect to MB in aqueous media [58]. Owing to these new electro kinetic characteristics, the adsorption capacity of MB on to this new adsorbent was found to increase significantly. This enhancement was attributed to the formation of negative surface charges as sodic sites: $\equiv X-O^- Na^+$ (with X = Al, Si, and Fe) which interact more favorably with cationic MB ions in water. Indeed, from electrochemical titration it was recently revealed by Allahdin et al. [59] that: (i) the addition of H_3O^+ solution into coated-brick suspensions could neutralize $\equiv X-O^-$ groups at the material surface; and (ii) at least two types of basic groups were detected, suggesting that Na atoms were bound not only to iron-oxihydroxide, as $\equiv FeO^-Na^+$, but also to other basic sites like $\equiv SiO^-Na^+$ and $\equiv Al^-Na^+$ from brick aluminosilicates (silanol and aluminol being generated through brick-metakaolinite hydroxylation by HCl treatment).

From these studies, it is nevertheless difficult to establish a quantitative relationship between the zeta potential (ζ) and the amount of MB adsorbed on to sand and brick particularly for two reasons: the surface potential is higher than ζ and the specific surface area of these two adsorbents differs significantly each other. However, when examining negative ζ values at initial batch-experiments pH as a function of MB adsorbed, a non-linear increase was obtained, confirming that the degree of increase in ζ upon adsorption corresponded to better affinity of MB molecules towards brick surfaces than sand surfaces.

CONCLUSIONS

In the present work, sand and brick from Bangui region were studied in terms of their removal of MB, a cationic dye pollutant. The experimental data obtained with sand and coated brick best fitted the Langmuir isotherm model. This fitting then revealed that the coverage of MB examined on the surface of sand and brick occurred according to a monolayer adsorption process.

Adsorption performances were found to be more related to the presence of hydroxyl and $-COO^-$ groups at the surfaces of the sand (organic matter) and brick (silanol and aluminol) than to the surface physical (BET) characteristics of these materials. Hydroxylation and dealumination of raw brick by acid activation allowed an increase of –OH functions at the solid surface, and subsequently, a deposition of iron oxihydroxide led to the generation of (ionizable) sodic surface sites: $\equiv X-O^-Na^+$, with X = Al, Si, and Fe. These chemical changes in surface brick were found to be the main reasons why the observed adsorbed amount of MB on to coated brick was higher than that on to raw brick. From electro kinetic measurements, it was demonstrated that (i) electrostatic attraction was the primary driving force at the solid – water interface for MB adsorption in our systems; and (ii) more negative zeta-potential values were obtained for coated brick across the whole pH range > pH_{IEP}. The enhancement in MB adsorption by coated brick was interpreted in terms of new

negative charges at the material surface. From this investigation, a conclusion could easily be drawn: an increase of the adsorption capacity would be due to the enforcement in electrostatic attraction between cationic MB and negatively charged adsorbent surfaces, mainly observed on the activated – brick material, with a strong implication of Na^+ ions and H^+ and OH^- potential – determining ions due to the exchanges at the brick – water interface.

ACKNOWLEGMENTS

This research was partly funded by the "Agence de l'Eau Artois-Picardie," the "Region Nord Pas-de-Calais," and the "Conseil Général du Nord," The study was part of Belvia Bagoua's master which was defended on September 2014 and Eric Foto's thesis which was defended on February 2015. These investigations were undertaken successfully owing to the cooperation between the University of Lille1 (France) and the University of Bangui (Central African Republic). These research works have been financially supported by the Embassy of France to Bangui. We greatly thank Mr. Marc Pelletier, Head of Analytical Laboratory from Lhoist society at Nivelles Belgium, for carrying out BET measurements.

REFERENCES

1. Gil, A., Assis, F.C.C., Albeniz, S., Korili, S.A. Removal of dyes from wastewaters by adsorption on pillared clays. Chemical Engineering Journal. 168: 1032-1040 (2011).
2. Rahman, A., Urabe, T., Kishimoto, N. Color removal of reactive procion dyes by clay adsorbents. Procedia Environmental Sciences. 17: 270-278 (2013).
3. Zhou, K., Zhang, Q., Wang, B., Liu, J., Wen, P., Gui, Z., Hu, Y. The integrated utilization of typical clays in removal of organic dyes and polymer nanocomposites. Journal of Cleaner Production. 81: 281-289 (2014).
4. Elmoubarki, R., Mahjoubi, F.Z., Tounsadi, H., Moustadraf, J., Abdennouri, M., Zouhri, A., El Albani, A., Barka, N. Adsorption of textile dyes on raw and decanted Moroccan clays: Kinetics, equilibrium and thermodynamics. Water Resources and Industry. 9: 16-29 (2015).
5. Visa, M., Bogatu, C., Duta, A. Simultaneous adsorption of dyes and heavy metals from multicomponent solutions using fly ash. 256: 5486-5491 (2010).
6. Sun, D., Zhang, X., Wu, Y., Liu, X. Adsorption of anionic dyes from aqueous solution on fly ash. Journal of Hazardous Materials. 181: 335-342 (2010).
7. Visa, M., Chelaru, A.M. hydrothermally modified fly ash for heavy metals and dyes removal in advanced wastewater treatment. Applied Surface Science. 303: 14-22 (2014).
8. Gao, M., Ma, Q., Lin, Q., Chang, J., Bao, W., Ma, H. Combined modification of fly ash with $Ca(OH)_2/Na_2FeO_4$ and its adsorption of Methyl Orange. Applied Surface Science. 359: 323-330 (2015).
9. Yahyaei, B., Azizian, S. Rapid adsorption of anionic dyes by ordered nanoporous alumina. Chemical Engineering Journal. 209: 589-596 (2012).
10. Yahyaei, B., Azizian, S. Rapid adsorption of binary dye pollutants onto the nanostructred mesoporous alumina. Journal of Molecular Liquids, 199: 88-95 (2014).

11. Shen, J., Li, Z., Wu, Y., Zhang, B., Li, F. Dentrimer-based preparation of mesoporous alumina nanofibers by electrospinning and their application in dye adsorption. Chemical Engineering Journal. 264: 48-55 (2015).

12. Duran-Jimenez, G., Hernandez-Montoya, V., Montes-Moran, M.A., Bonilla-Petriciolet, A. Rangel-Vazquez, N.A. Adsorption of dyes with different molecular properties on activated carbons prepared from lignocellulosic wastes by Taguchi method. Microporous and Mesoporous Materials. 199: 99-107 (2014).

13. Georgin, J., Dotto, G.L., Mazutti, M.A., Foletto, E.L. Preparation of activated carbon from peanut shell by conventional pyrolysis and microwave irradiation-pyrolysis to remove organic dyes from aqueous solutions. Journal of Environmental Chemical Engineering. 4: 266-275 (2016).

14. Aguiar, J.E., de Oliveira, J.C.A., Silvino, P.F.G., Neto, J.A., Silva Jr., I.A., Lucena, S.M.P. Correlation between PSD and adsorption of anionic dyes with different molecular weigths on activated carbon. Colloids and Surfaces A: Physicochem. Eng. Aspects. 496: 125-131 (2016).

15. Liu, F., Guo, Z., Ling, H., Huang, Z., Tang, D. Effect of pore structure on the adsorption of aqueous dyes to ordered mesoporous carbons. Microporous and Mesoporous Materials. 227: 104-111 (2016).

16. Liao, P., Ismael,Z.M., Zhang, W., Yuan, S., Tong, M., Wang, K., Bao, J. Adsorption of dyes from aqueous solutions by microwave modified bamboo charcoal. Chemical Engineering Journal. 195-196: 339-346 (2012).

17. Rosales, E., Meijide, J., Tavares, T., Pazos, M., Sanroman, M.A. Grapefruit peelings as a promising biosorbent for the removal of leather dyes and hexavalent chromium. Process Safety and Environmental Protection. In press.

18. Kuppusamy, S., Thavamani, P., Megharaj, M., Venkateswarlu, K., Lee, Y.B., Naidu, R. Potential of *Melaleuca diosmifolia* as a novel, non-conventional and low-cost coagulating adsorbent for removing both cationic and anionic dyes. Journal of Industrial and Engineering Chemistry. In press.

19. Chan, S.L., Tan, Y.P., Abdullah, A.H., Ong, S.T. Equilibrium, kinetic and thermodynamic studies of a new potential biosorbent for the removal of Basic Blue 3 and Congo Red dyes: Pineapple (Ananas *comosus*) plant stem. Journal of the Taiwan Institute of Chemical Engineers. 61: 306-315 (2016).

20. Javadian, H., Angaji, M.T., Naushad, M. Synthesis and characterization of polyaniline/ γ-alumina nanocomposite: A comparative study for the adsorption of three different anionic dyes. Journal of Industrial and Engineering Chemistry. 20: 3890-3900 (2014).

21. Xiao, L., Xiong, Y., Tian, S., He, C., Su, Q., Wen, Z. One-dimensional coordination supramolecular polymer $[Cu(bipy)(SO_4)]_n$ as an adsorbent for adsorption and kinetic separation of anionic dyes. Chemical Engineering Journal. 265: 157-163 (2015).

22. Mahida, V.P., Patel, M.P. Superabsorbent amphoteric nanohydrogels: Synthesis, characterization and dyes adsorption studies. Chinese Chemical Letters. 27: 471-474 (2016).

23. Fu, J., Xin, Q., Wu, X., Chen, Z., Yan, Y., Liu, S., Wang, M., Xu, Q. Selective adsorption and separation of organic dyes from aqueous solution on polydopamine microspheres. Journal of Colloid and Interface Science. 461: 292-304 (2016).

24. Li, Y., Nie, W., Chen, P., Zhou, Y. Preparation and characterization of sulfonated poly(styrene-alt-maleic anhydride) and its selective removal of cationic dyes. Colloids and Surfaces A: Physicochemical and Engineering Aspects. 499: 46-53 (2016).

25. Tyagi, V.K., Khan, A.A., Kazmi, A.A., Mehrotra, I., Chopra, A.K. Slow sand filtration of UASB reactor effluent: A promising post treatment technique. Desalination. 249: 571-576 (2009).

26. Gherairi, Y., Amrane, A., Touil, Y., Hadj Mahammed, M., Gherairi, F., Baameur, L. A comparative study of the addition effect of activated carbon obtained from date stones on the biological filtration efficiency using sand dune bed. Energy Procedia. 36: 1175-1183 (2013).

27. Bori Akadar, A., Bourioug, M., Mohamed, N., Badr, A.S., Cavalli, E., Lotfi, A. Wastewater use in agriculture in Djibouti: Effectiveness of sand filtration treatments and impact of wastewater irrigation on growth and yield of *Panicum maximum*. Ecological Engineering. 84: 607-614 (2015).

28. Taqvi, S.I.H., Hasany, S.M., Bhanger, M.I. Sorption profile of Cd(II) ions onto beach sand from aqueous solutions. Journal of Hazardous Materiauls. 141: 37-44 (2007).

29. Rauf, M.A., Iqbal, M.J., Ellahli, I., Hasany, S.M. Kinetic and thermodynamic aspects of ytterbium adsorption on sand. Adsorp. Sci. Technol. 13: 97-104 (1996).

30. Bukallah, S.B., Rauf, M.A., AlAli, S.S. Removal of Methylene Blue from aqueous solution by adsorption on sand. Dyes Pigments. 74: 85-87 (2007).

31. Rauf, M.A., Shehadi, I.A., Hassan, W.W. Studies on the removal of Neutral Red on sand from aqueous solution and its kinetic behavior, Dyes Pigments. 75:723-726.

32. Rauf, M.A., Bukallah, S.B., Hamour, F.A., Nasir, A.S. Adsorption of dyes from aqueous solutions onto sand and their kinetic behavior. Chemical Engineering Journal. 137: 238-243 (2008).

33. Boujelben, N., Bouzid, J., Elouear, Z., Feki, M., Jamoussi, F., Montiel, A. Phosphorus removal from aqueous solution using iron coated natural and engineered sorbents. Journal of Hazardous Materials 151 (2008) 103-110.

34. Selvaraju, N., Pushpavanam, S. Adsorption characteristics on sand and brick beds. Chemical Engineering Journal. 147: 130-138 (2009).

35. Bina, R., Raaz, M., R., Chauhan, A.K., Bhaskar, N.S. Defluoridation of contaminated water employing brick powder as an adsorbent. International Journal of Science and Nature. IJSN-Vol.3(1): 78-82 (2012).

36. Labidi, N.S. Removal of mercury from aqueous solutions by waste brick. International Journal of Environmental Research 2(3): 275-278 (2008).

37. Witharana, A., Jayaweera, M., Manatunge, J. Zinc adsorption by low cost sorbent materials: Clay tile, brick, sawdust and rice husk. International Conference on Sustainable Built Environment (ICSBE-2010). Kandy, 13-14 December 2010, pp. 21-28.

38. Gandhi, N., Sirisha, D., Chandra Sekhar, K.B. Adsorption studies of chromium by using low cost adsorbents. Our

Nature 11(1): 11-16 (2013).

39. Hemalatha, P.V., Prasada Rao, P.V.V. Adsorption batch studies on calcined brick powder in removing chromium and nickel ions. International Journal of Advanced Research in Chemical Science. 1(6): 14-21 (2014),.
40. Hema Krishna, R., Swamy, A.V.V.S. Physico-chemical key parameters, Langmuir and Freundlich isotherm and Lagergren rate constant studies on the removal of calcined brick. International Journal of Engineering Research and Development. 4(1): 29-38 (2012).
41. Hamdaoui, O. Batch study of liquid-phase adsorption of methylene blue using cedar sawdust and crushed brick. Journal of Hazardous Materials. 135: 264-273 (2006).
42. Hamdaoui, O. Dynamic sorption of methylene blue by cedar sawdust and crushed brick in fixed bed columns. Journal of Hazardous Materials. B138: 293-303 (2006).
43. Kooli, F., Yan, L., Al-faze, R., Al-Sehimi, A. Removal enhancement of basic blue 41 by brick waste from an aqueous solution. Arabian Journal of Chemistry. 8: 333-342 (2015).
44. Crittenden, J.C., Trussell, R.R., Hand, D.W., Howe, K.J., Tchobanoglous, G. MWH's Water Treatment: Principles and Design. Wiley. Hoboken, 2012.
45. Edzwald, J.K. Water Quality & Treatment: A Handbook on Drinking Water. McGraw-Hill, New York, NY, 2011.
46. Muzzarelli, R.A.A., Muzzarelli, C. Chitosan chemistry: relevance to the biomedical sciences. Adv. Polym. Sci. 186: 151-209 (2005).
47. Chen, R., Zhang, Y., Shen, L., Wang, X., Chen, J. Ma, A. Jiang, W. Lead(II) and methylene blue removal using a fully biodegradable hydrogel based on starch immobilized humic acid. Chemical Engineering Journal. 268: 348-355 (2015).
48. Allahdin, O., Wartel, M., Tricot, G., Revel, B., Boughriet, A. Hydroxylation and dealumination of a metakaolinite-rich brick under acid conditions, and their influences on metal adsorption: One- and two-dimensional (^{1}H, ^{27}Al, ^{23}Na, ^{29}Si) MAS NMR, and FTIR studies. Microporous and Mesoporous Materials. 226: 360-368 (2016).
49. Malfait, W.J., Xue, X. The nature of hydroxyl groups in aluminosilicate glasses: Quantifying Si–OH and Al–OH abundances along the SiO_2-$NaAlSiO_4$ join by ^{1}H, ^{27}Al–^{1}H and ^{29}Si–^{1}H NMR spectroscopy. Geochimica ET Cosmochimica Acta. 74: 719-737 (2010).
50. Malfait, W.J., Xue, X. The partial ^{1}H NMR spectra of Al–OH and molecular H_2O in hydrous aluminosilicate glasses: Component-resolved analysis of ^{27}Al–^{1}H cross polarization and ^{1}H spin-echo MAS NMR spectra. Solid State Nuclear Magnetic Resonance. 37: 60-68 (2010).
51. Kim, H.N., Lee, S.K. Atomic structure and dehydration mechanism of amorphous silica: Insights from ^{29}Si and ^{1}H solid-state MAS NMR study of SiO_2 nanoparticles. Geochimica ET Cosmochimica Acta. 120: 39-64 (2013).
52. Cismasu,A.C., Levard, C., Michel, F.M., Brown Jr., G.E. Properties of imputity-bearing ferrihydrite II: Insights

into the surface structure and composition of pure, Al- and Sibearing ferrihydrite from Zn(II) sorption experiments and Zn K-edge X-ray absorption spectroscopy. Geochimica et Cosmochimica Acta. 119: 46-60 (2013).

53. Zhou, Y., Zhang, Y., Li, P., Li, G., and Jiang, T. Comparative study on the adsorption interactions of humic acid onto natural magnetite, hematite, and quartz: Effect of initial HA concentration. Powder Technology 251: 1-8 (2014).
54. Zhou, Y., Zhang, Y., Li, G., Wu, Y., Jiang, T. A further study on adsorption interaction of humic acid on natural magnetite, hematite and quartz in iron ore pelletizing process: Effect of the solution pH value. Powder Technology 271: 155-166 (2015).
55. Jin, J., Gao, H., Chen, X., Peng, Y. The separation of kyanite from quartz by flotation at acidic pH. Minerals Engineering. 92: 221-228 (2016).
56. Kosmulski, M. Compilation of PZC and IEP of sparingly soluble metal oxides and hydroxides from literature. Advances in Colloid and Interface Science. 152: 14-25 (2009).
57. Huertas, F.J., Chou, L., Wollast, R. Mechanism of kaolinite dissolution at room temperature and pressure: Part 1. Surface speciation. Geochimica ET Cosmochimica Acta. 62: 417-431 (1998) and references therein.
58. Cottet, L., Almeida, C.A.P., Naidek, N., Viante, M.F., Lopes, M.C., Debacher, N.A. Adsorption characteristics of montmorillonite clay modified with iron oxide with respect to methylene blue in aqueous media. Applied clay Science. 95: 25-31 (2014).
59. Allahdin, O., Bagoua, B., Wartel, M., Mabingui, J., Boughriet, A. Effects of chemical activation on surface sites of the brick: pH-dependence on metal adsorption. International Journal of New Technology and Research. 2(1): 22-31 (2016).